Chiral diethyl-EDT-TTF and tetraethyl-BEDT-TTF: synthesis, structural characterization, radical cation salt and charge transfer complexes

Nabil Mroweh, Thomas Cauchy, Nicolas Vanthuyne, Narcis Avarvari

Chiral diethyl-EDT-TTF and tetraethyl-BEDT-TTF: synthesis, structural characterization, radical cation salt and charge transfer complexes

Nabil Mroweh,[a] Thomas Cauchy,[a] Nicolas Vanthuyne,[b] and Narcis Avarvari*[a]

[a] *Univ Angers, CNRS, MOLTECH-Anjou, SFR MATRIX, F-49000 Angers, France. E-mail: narcis.avarvari@univ-angers.fr*

[b] *Aix Marseille Université, CNRS, Centrale Marseille, iSm2, Marseille, France.*

Abstract

The chiral electroactive precursors diethyl-ethylenedithio-tetrathiafulvalene (DE-EDT-TTF **1**) and tetraethyl-bis(ethylenedithio)-tetrathiafulvalene (TE-BEDT-TTF **2**) have been synthesized in the racemic form and separated in pure enantiomers, together with the *meso* form of **2**, by chiral HPLC. All the neutral forms (*rac*)-, (*S*)- and (*R*)-**1**, (*rac*)-, (*S*)-, (*R*)- and (*meso*)-**2** have been structurally characterized by single crystal X-ray diffraction analysis. In all the structures the ethyl substituents are in axial positions, in agreement with the results of the DFT calculations, which indicate that the axial conformation of the ethyl substituents of **1** is more stable by 0.95 kcal/mol than the equatorial conformation in the gas phase. Circular dichroism measurements combined with TD-DFT calculations are also in favour of the predominance of the axial conformers in solution. The crystalline radical cation salt [(*S*)-**1**]PF_6 and charge transfer complexes [(*R*)-**1**]$TCNQF_4$ and [(*meso*)-**2**]$TCNQF_4$ have been structurally characterized. A segregated donor-acceptor structure is observed for [(*R*)-**1**]$TCNQF_4$, while in [(*meso*)-**2**]$TCNQF_4$ donors and acceptors alternate in the stacks.

1. Introduction

The ever growing interest for chiral conducting materials[1] relies either on the synergistic effect between chirality, electron conductivity and magnetic field referred to as electrical magnetochiral anisotropy (eMChA),[2] on the modulation of the conducting properties between enantiopure and racemic forms as a consequence of the structural disorder[3,4] or of the different crystalline packing,[5,6] or on the possible occurrence of a selective spin transmission through the so-called chirality induced spin selectivity (CISS) effect,[7,8] recently observed in the linear transport regime.[9] Therefore several families of chiral electroactive molecular precursors have been developed in this respect,[1,10] the vast majority being based on the tetrathiafulvalene (TTF) unit.[11] Methylated bis(ethylenedithio)-tetrathiafulvalene (BEDT-TTF) and ethylenedithio-tetrathiafulvalene (EDT-TTF) derivatives, such as tetramethyl-BEDT-TTF (TM-BEDT-TTF), dimethyl-BEDT-TTF (DM-BEDT-TTF) and dimethyl-EDT-TTF (DM-EDT-TTF) (Scheme 1), represent to date the most extensively used chiral tetrathiafulvalene (TTF) precursors for chiral conducting radical cation salts or charge transfer complexes.[1] Indeed, TM-BEDT-TTF, which was the first reported enantiopure TTF derivative,[12,13] provided, for example, various radical cation salts such as (TM-BEDT-TTF)$_3$(XO$_4$)$_2$ (X = Cl, Re),[14] (TM-BEDT-TTF)$_2$XF$_6$ (X = P, As, Sb),[15] (TM-BEDT-TTF)$_x$[MnCr(ox)$_3$] (ox = oxalate),[16] (TM-BEDT-TTF)[(*rac*)-TRISPHAT],[17] (TM-BEDT-TTF)I$_3$,[18] (TM-BEDT-TTF)$_3$(PPh$_4$)[KFe(Cl$_2$An)$_3$] (Cl$_2$An = dichloroanilate),[19] (TM-BEDT-TTF)$_2$(Re$_6$S$_6$Cl$_8$),[20] or [TM-BEDT-TTF]$_9$(Mo$_6$O$_{19}$)$_5$,[21] showing semiconducting and/or metallic behaviour. On the other hand, DM-BEDT-TTF, besides the semiconducting salts (DM-BEDT-TTF)$_2$X (X = PF$_6$, ClO$_4$, ReO$_4$)[22] and (DM-BEDT-TTF)$_2$(ReCl$_6$),[23] afforded the metallic phase κ-[(*S*,*S*)-DM-BEDT-TTF]$_2$ClO$_4$,[24] which was initially described as superconducting at low temperature under pressure, yet this claim has been recently challenged.[25] Finally, DM-EDT-TTF provided salts such as (DM-EDT-TTF)$_2$(XF$_6$) (X = P, As, Sb),[5,6] where the occurrence of metallic *versus* semiconducting behaviour depends on the size of the anion, (DM-EDT-TTF)$_3$(Ta$_2$F$_{10}$O)[26] and, particularly, (DM-EDT-TTF)$_2$ClO$_4$,[27] which allowed the first observation of the eMChA effect in a bulk chiral crystalline conductor. More recently, we have described the monomethyl analogue Me-EDT-TTF (Scheme 1), containing only one stereogenic centre, together with several radical cation salts.[28,29,30] In order to study the influence of the steric hindrance brought by the alkyl substituent, the slightly bigger precursor Et-EDT-TTF (Scheme 1) has been prepared as well.[28] Completely different crystalline structures have been observed for the two donors,

both in the neutral precursors and the corresponding salts, when going from the methyl to the ethyl substituent.[28,29] As a continuation of our endeavour in the field of chiral electroactive precursors, we describe herein the synthesis, chiral separation and chiroptical and structural characterization of the DE-EDT-TTF (**1**) and TE-BEDT-TTF (**2**) donors (Scheme 1), together with a radical cation salt and two charge transfer complexes. Note that TE-BEDT-TTF was previously reported in 1999 by Kini et al.,[31] as a mixture of racemic and meso forms.

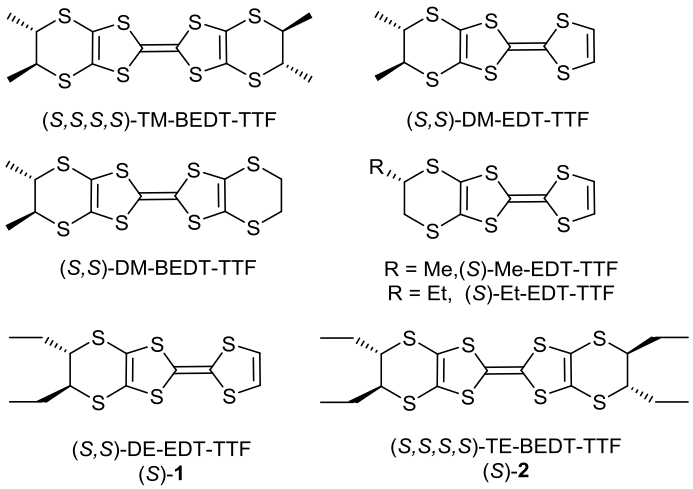

Scheme 1 Enantiopure BEDT-TTF and EDT-TTF based donors; DE-EDT-TTF (**1**) and TE-BEDT-TTF (**2**) are described in this work.

2. Results and discussion

2.1 Synthesis and chiroptical properties of the neutral donors 1 and 2

The donors **1** and **2** have as common precursor the 5,6-diethyl-5,6-dihydro-1,4-dithiin-2,3-dithiol-thione half **5**, obtained as racemic form upon a slightly modified procedure[31] involving the hetero Diels-Alder [4+2] cycloaddition between 1,3-dithiole-2,4,5-trithione **4**, conveniently prepared from the $(Et_4N)_2[Zn(dmit)_2]$ complex **3**, and *trans*-3-hexene (Scheme 2). Then, the "classical" phosphite mediated heterocoupling between **5** and the 4,5-dimethylcarboxylate-1,3-dithiol-2-one **6** afforded concomitantly the homo-coupled TE-BEDT-TTF **2**, obtained as a mixture of racemic (*S*,*S*,*S*,*S*)/(*R*,*R*,*R*,*R*) and meso (*S*,*S*,*R*,*R*) compounds, the tetraester-TTF **8** and the hetero-coupled DE-EDT-TTF-diester **7** as racemate, the three compounds being readily separated by chromatography on silica-gel column. The diester **7** was further subjected to a double decarboxylation affording racemic DE-EDT-TTF **1**. As mentioned above, the TE-BEDT-TTF **2** was previously prepared *via* the phosphite mediated homocoupling of the dithiolone version of **5**, yet no attempts of chiral separation

were mentioned, and thus it was further used in electrocrystallization experiments as (*rac*)/(*meso*) mixtures.[31]

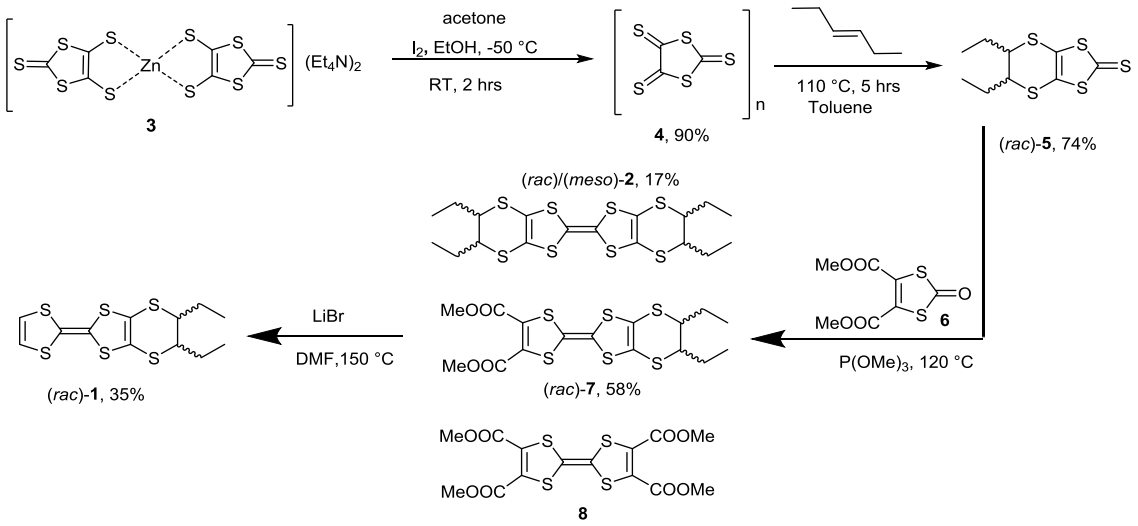

Scheme 2 Synthesis of racemic DE-EDT-TTF (**1**) and racemic/meso TE-EDT-TTF (**2**).

The analytical and electrochemical characterization of **2** are in agreement with the published data,[31] while cyclic voltammetry measurements of **1** show the characteristic pair of reversible oxidation processes occurring at $\Delta E_{1/2}$= +0.42 and 0.74 V *vs* SCE for the generation of the radical cation and of the dication, respectively (see Fig. S1, ESI).

Both donors have been successfully separated as pure enantiomers (*S*,*S*) and (*R*,*R*) for **1** and (*S*,*S*,*S*,*S*) and (*R*,*R*,*R*,*R*) together with the meso form (*S*,*S*,*R*,*R*) for **2**, by semi-preparative chiral HPLC on Chiralpak IG column (Figs. S2-S5 for **1** and Figs. S6-S11 for **2**, ESI). Note that two successive separations were required for compound **2** in order to have the pure enantiomers and the meso diastereoisomer (ESI). The optical rotations, circular dichroism (CD) and UV-Vis absorption spectra were measured for the two pairs of enantiomers of **1** and **2**, abbreviated hereafter (*S*)-**1**/(*S*)-**2** and (*R*)-**1**/(*R*)-**2** (ESI). The absolute configurations for (*S*)-**1**/(*R*)-**1** and (*S*)-**2**/(*R*)-**2**, respectively, have been attributed by comparison with the specific optical rotations and the CD spectra of DM-EDT-TTF[32] and TM-BEDT-TTF,[18] for which the all-axial conformers were found to be predominant in solution, in agreement with the DFT calculations. Accordingly, (*S*)-**1** and (*S*)-**2** enantiomers are levorotatory, with specific optical rotation values of -188 and -202 deg·mL·g^{-1}·dm^{-1} ($[\alpha]_D^{25}$ in CH_2Cl_2), respectively, while the CD spectra show one weak negative, one weak positive, one medium intense negative and one medium intense positive bands peaking at 365 nm, 313 nm, 274 nm and 227 nm for (*S*)-**1** and two weak negative, one weak positive, one medium intense negative and one medium

intense positive bands peaking at 369 nm, 352 nm, 314 nm, 270 nm and 225 nm for (*S*)-**2**. Mirror-image CD spectra were obtained for the (*R*) enantiomers which are dextrotatory (Figs. S5 and S11, ESI). The CD spectra of **1** and **2** present similar patterns to those of DM-EDT-TTF[32] and TM-BEDT-TTF,[18] respectively, strongly suggesting the predominance of the all-axial conformers in solution, which were found to be more stable than the all-equatorial ones when the two carbon atoms of the ethylenedithio bridge are substituted.

2.2 DFT and TD DFT calculations on donor 1

In the case of donor **1**, the two stable conformers (ax,ax) and (eq,eq) for the (*S*) enantiomer are represented in Scheme 3.

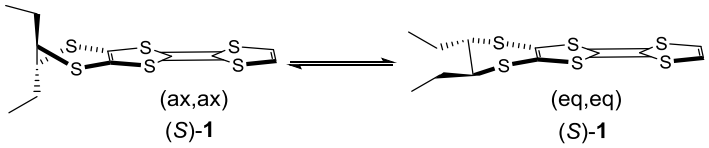

Scheme 3 The two stable conformers of (*S*)-DE-EDT-TTF.

In order to estimate the relative stability of these two conformers, DFT and TD-DFT calculations have been carried out for the compound **1** for both enantiomers. The gas phase calculated Gibbs free energies confirm indeed that the (ax,ax) conformation is more stable than the (eq,eq) one by at least 0.95 kcal/mol, a value which is more than 40% higher than in the case of DM-EDT-TTF.[32] This energy difference correspond to a Boltzmann ratio of almost 5 (ax,ax) for 1 (eq,eq). Thus, the predominance of the (ax,ax) conformation of **1** in solution and, probably, in the solid state, over the (eq,eq) one occurs at a much larger extent than in DM-EDT-TTF. This result represents an important consequence of the influence of the steric hindrance of the substituents on the conformational stability of the doubly substituted EDT bridge in EDT-TTF derivatives. The energy difference also explains the experimental CD spectra of **1** discussed above. In Fig. 1 are reported the experimental spectra for (*R*)-**1** and (*S*)-**1** as well as the theoretical curves based on TD-DFT calculations on the (ax,ax) conformers. The properties of the (eq,eq) conformers are available in the full molecular report in the supplementary information.

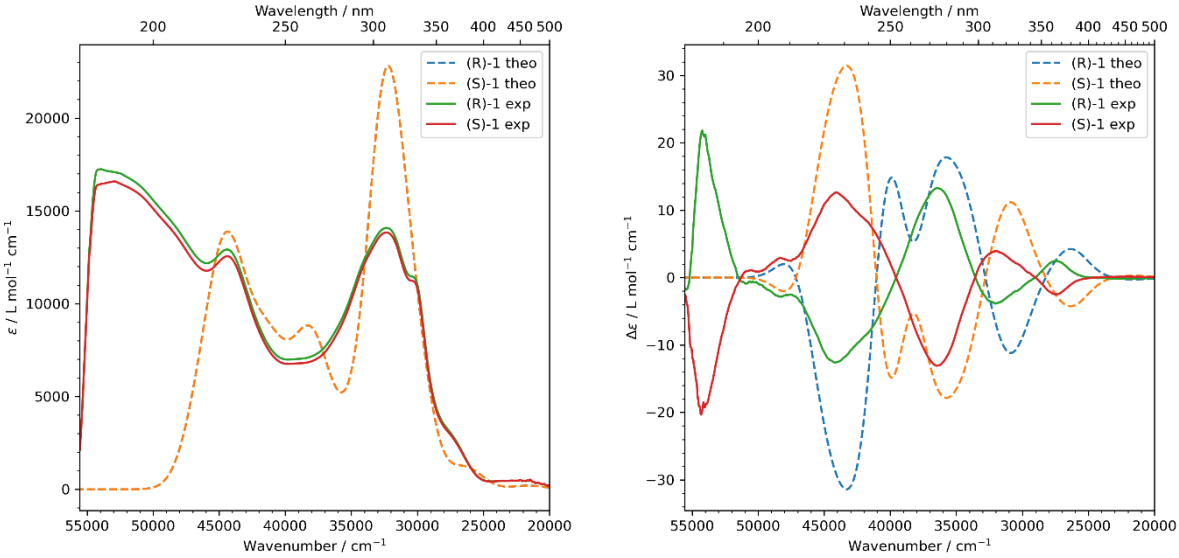

Fig. 1 Experimental (lines) and calculated (dashed lines) UV-visible absorption spectra (left) and circular dichroism spectra (right) for (*R*)-**1** and (*S*)-**1.** The calculated curves correspond to the (ax,ax) conformers and have been obtained with a Gaussian broadening (FWHM = 3000 cm^{-1}).

The electron density differences associated to each transitions calculated by TD-DFT allow for a nice rationale of the absorption and circular dichroism properties. The most significant electron density differences are reported in Fig. 2. For the absorption spectra, the large band around 300 nm is mainly due to the $S_0 \rightarrow S_6$ transition. The high absorption intensity of this transition is due to its C=C π to π* nature as shown by the electron loss (white surface) located in two of the three C=C bonds. Concerning the circular dichroism, a slight red shift is observed between the experimental and the (ax,ax) theoretical curves. The agreement even up to 220 nm support the predominance of the (ax,ax) conformation in solution. The first negative band of (*S*)-**1** is due to S_2 and correspond to the loss of electron density in the TTF core to the outer π* C=C bonds. The dichroism signal is weak as the EDT show a small contribution in the transition. The positive band at 310 nm and the negative band at 270 nm are composed of different transitions but their main contributors are respectively S_4 and S_{13}. In both cases the inner core of the TTF, i.e. the central C=C bond and the four conjugated electron lone pairs of the four sulphur atoms, loose electron density to enrich the EDT part. The huge surfaces indicate some contribution of Rydberg states as expected in high-energy transitions. One can notice that intense dichroism signals are indeed associated with electron density transfer on the stereocenters.

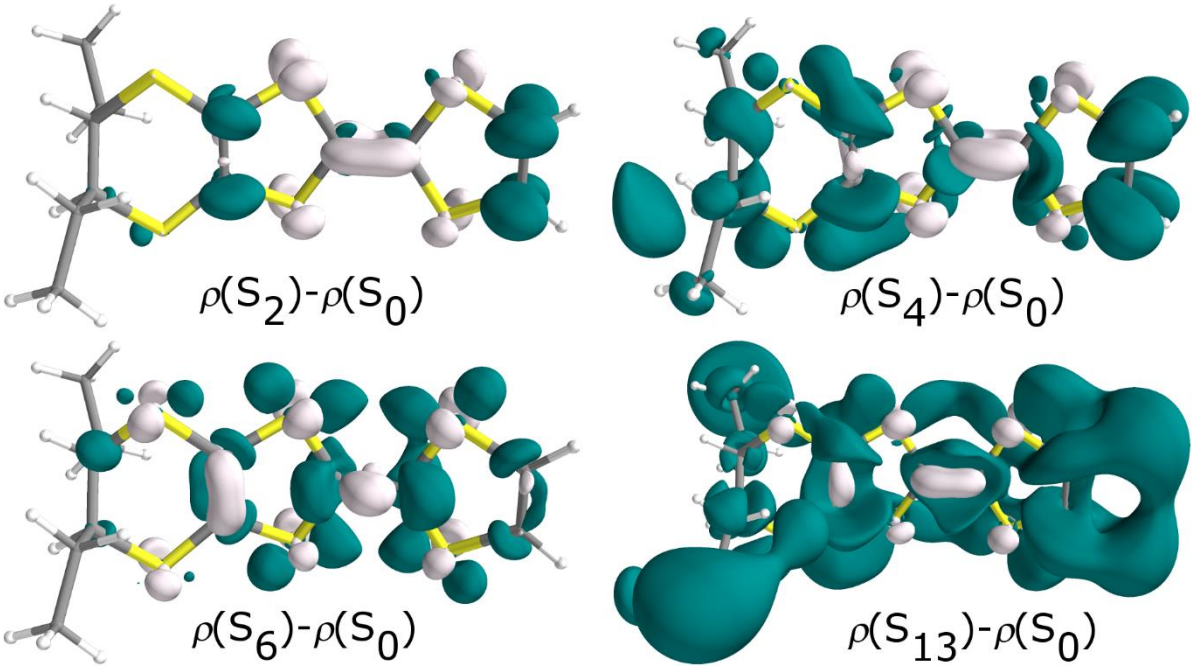

Fig. 2 Representation of the electron density difference (EDD) of the most significant calculated transitions of (*S*)-**1** (ax,ax) conformer. The blue surface represents the excited electron (electron density gain upon excitation) and the white surface the hole.

2.3 Crystalline structures of the neutral donors 1 and 2

The assignment of the absolute configuration of the enantiopure donors **1** and **2** was also confirmed by single crystal X-ray analysis (Tables S1 and S2, ESI). Single crystals of (*S*)-**1** and (*R*)-**1** have been obtained as brown orange plates by slow evaporation of solutions in methylene chloride. The two enantiomers are isostructural, crystallizing in the monoclinic non-centrosymmetric $P2_1$ space group with one independent molecule in the unit cell (Fig. 3 for (*S*)-**1** and Fig. S12 for (*R*)-**1**).

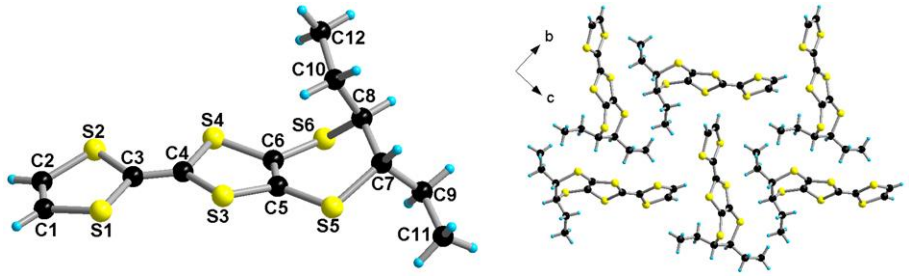

Fig. 3 Molecular structure of (*S*)-**1** together with the atom numbering scheme (left) and a packing diagram in the *bc* plane side view (right).

The dithiin six-membered ring shows a boat-like conformation[13] (dihedral angles C5-C6-S6-C7 and C6-C5-S5-C8 equal -18.1° and 30.5° respectively) with axial (ax) orientations of the ethyl substituents, and boat-like conformation of the TTF unit, with slight distortions around

the internal S···S axes of 11.3 and 15.8°, opposite to that of the dithiin ring. The existence of the (ax,ax) conformer in the solid state is in line with the results on DM-EDT-TTF, which was also found in the crystal structure as (ax,ax) conformer.[5] This was calculated to be slightly more stable than the conformer with equatorial (eq) orientations of the methyl substituents.[32] In the packing, the donors arrange in an orthogonal manner to each other in the *bc* plane, and form chains along the *a* direction with intermolecular S···S distances over 3.8 Å.

Single crystals of (*rac*)-**1** were obtained by crystallization in DMSO as dark brown needles. The compound crystallizes in the polar non-centrosymmetric orthorhombic *P*na2_1 space group, with a Flack parameter of 0.03(3). The unit cell contains two independent donor molecules in the unit cell, A and B (both of them have (*R*) configuration in Fig. S13). The dithiin six-membered rings show sofa type conformations (dihedral angles -7.5 and -6.2° for molecule A and -3.3 and -8.6° for molecule B), with axial orientation of the ethyl substituents, and boat-like conformation of the TTF unit. The packing is very similar to the one observed in the crystals obtained starting from the pure enantiomers, with the donor molecules orthogonal to each (Fig. S13). The central C=C and internal C−S bond distances have typical values for neutral donors (Table S3).

Suitable single crystals for X-ray analysis for the different forms of neutral **2**, i.e. racemic, enantiopure and meso, have been obtained upon slow evaporation of either a toluene solution of (*rac*)-**2** or of the solutions after the HPLC separation, typically heptane / methylene chloride / ethanol mixtures, for the other compounds. In the previous report by Kini et al. the structure of (*rac*)-**2**, which crystallized out of the (*rac*)/(*meso*) mixture in the chiral tetragonal non-centrosymmetric space group $P4_32_12$, has been already reported.[31] As the authors mentioned, the compound spontaneously resolved upon crystallization in equal amounts of enantiomorphic $P4_32_12$ and $P4_12_12$ crystals. Interestingly, the crystal we have analysed pertains to the $P4_12_12$ space group, containing two half independent (*S*) and (*R*) molecules in the unit cell located on C_2 symmetry axes (Fig. 4).

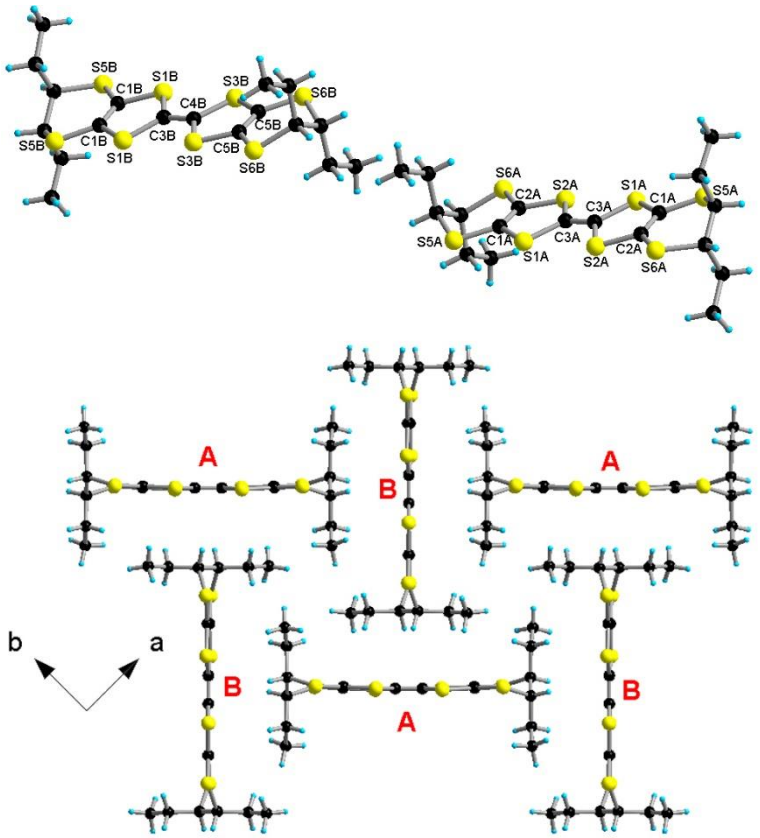

Fig. 4 The two independent molecules in the crystal structure of (*rac*)-**2** along with a partial atom numbering scheme (top); packing diagram in the *ab* plane showing the orthogonal arrangement of the A and B independent molecules (bottom).

At the difference with the previously reported structure in the $P4_32_12$ group,[31] the molecule located on the C_2 axis encompassing its longitudinal dimension is now the one of (*R*) configuration (molecule B), while the one with the C_2 axis perpendicular to its mean plane is of (*S*) configuration (molecule A). As in the case of DE-EDT-TTF **1** (see Fig. 2), the ethyl substituents are oriented in axial positions, at the difference with the TM-BEDT-TTF donor (see Scheme 1) for which the conformer which crystallizes more readily is the all-eq one,[18] although the all-ax one could be also crystallized in particular conditions.[15] This difference is very likely related to the higher stability of the all-ax conformer with respect to the all-eq one for donor **2** compared to TM-BEDT-TTF. The A and B molecules are orthogonal to each other in the *ab* plane, as a consequence of the tetragonal symmetry of the lattice (Fig. 4).

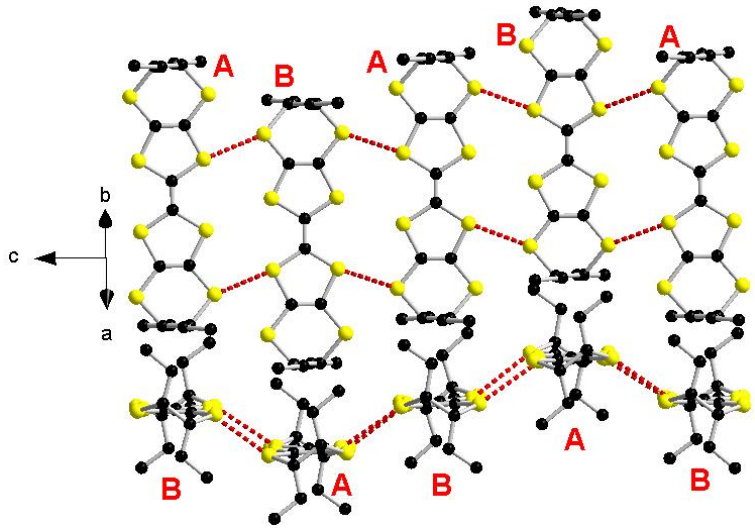

Fig. 5 Packing diagram of (*rac*)-**2** along the *c* direction. The highlighted S···S intermolecular distances (red dotted lines) amount to 3.47 – 3.48 Å.

The donors form corrugated ribbons along the *c* direction with an alternation of the A and B molecules which engage in intermolecular interactions with rather short S···S distances (3.47 – 3.48 Å) (Fig. 5). Adjacent ribbons are perpendicular to each other and are separated by the alkyl ends of the molecule.

The enantiopure forms (*S*)-**2** and (*R*)-**2** crystallized in the monoclinic non-centrosymmetric space group $P2_1$, with only one independent molecule in the unit cell (Figs. 6 and S14 for (*S*)-**2** and Figs. S15-16 for (*R*)-**2**). Since the two enantiomers are crystallographically isostructural, only the structure of (*S*)-**2** will be discussed in the following. The four ethyl substituents are located in axial positions and the overall shape of the molecule is boat-like because of the strong folding around the internal S···S hinges, with dihedral angles of 23° (S1···S2) and 30.1° (S3···S4) (Fig. 6, see also Fig. S15 for (*R*)-**2**). Note that in the structure of (*rac*)-**2** (*vide supra*) the donors are planar.

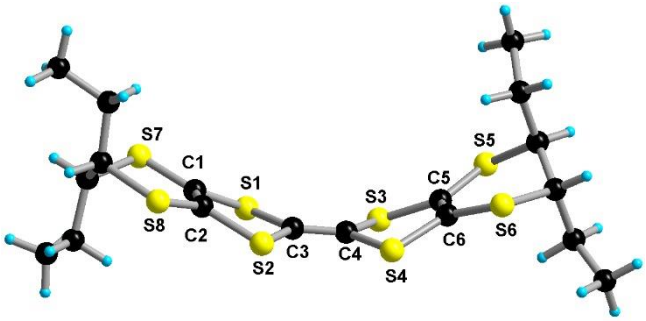

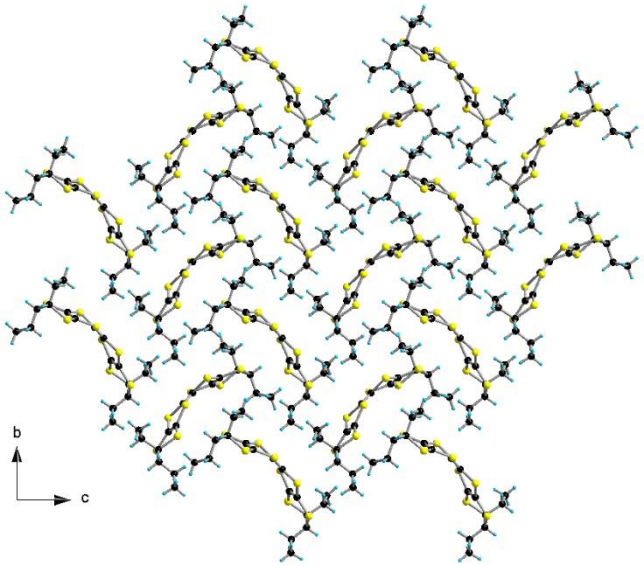

Fig. 6 Molecular structure of (*S*)-**2** along with a partial atom numbering scheme (top); packing diagram in the *bc* plane showing the orthogonal arrangement of the molecules (bottom).

Interestingly, in spite of the different crystal parameters when compared to (*rac*)-**2**, the donors pack again in an orthogonal manner, in the *bc* plane (Fig. 6 and Fig. S15 for (*R*)-**2**), and establish ribbons along the *a* direction with the shortest S···S intermolecular contact amounting to 3.77 Å for (*S*)-**2** (Fig. S14) and 3.70 Å for (*R*)-**2** (Fig. S16).

Finally, the meso compound (*meso*)-**2** crystallized in the centrosymmetric monoclinic space group $P2_1/c$ with one half independent molecule in the asymmetric unit, located on an inversion centre (Fig. 7). As in the previous cases, the ethyl substituents are in axial positions and the donors are arranged orthogonal to each other in the *bc* plane (Fig. 7). The donor molecule is not fully planar, but slightly folded around the S1···S2 axis with a dihedral angle of 7.6° within a chair-like conformation of the central TTF core.

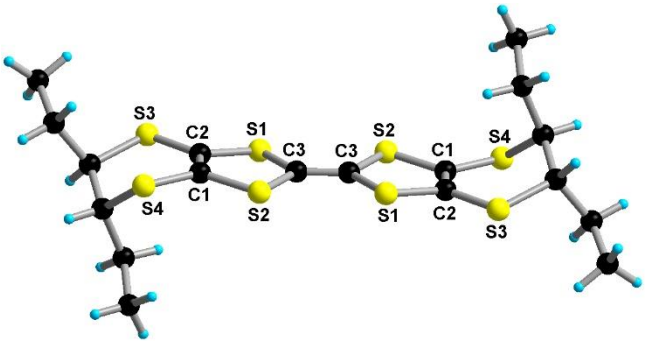

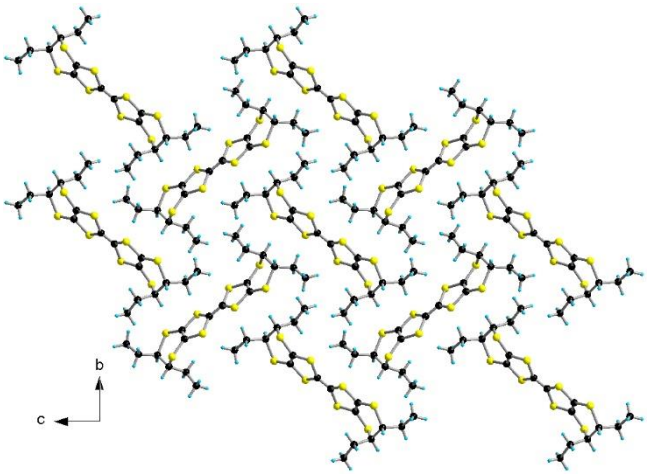

Fig. 7 Molecular structure of (*meso*)-**2** along with a partial atom numbering scheme (top); packing diagram in the *bc* plane showing the orthogonal arrangement of the molecules (bottom).

The shortest S···S intermolecular contacts are observed between donors along the *a* direction, leading to the formation of stair-chase ribbons (Fig. S17). The central C=C and internal C−S bond distances have typical values for neutral donors (Table S4).

2.4 Crystalline structures of the radical cation salts and charge transfer complexes

Although both donors **1** and **2** have been engaged in numerous electrocrystallization attempts, only those concerning the donor **1** in combination with [(*n*-Bu)$_4$N]PF$_6$ as supporting electrolyte afforded crystalline radical cation salts formulated as (**1**)PF$_6$. The enantiomeric salts [(*S*)-**1**]PF$_6$ and [(*R*)-**1**]PF$_6$ are isostructural and crystallize in the non-centrosymmetric triclinic space group *P*1, while the racemic salt [(*rac*)-**1**]PF$_6$ crystallizes in the centrosymmetric space group *P*-1 with the same cell parameters. However, only crystals of the (*S*) enantiomer provided high quality X-ray diffraction data, therefore only the structure of [(*S*)-**1**]PF$_6$ will be detailed hereafter (Table S1). There are four independent donors (A-D) and four anions (P1-P4) in the unit cell (Fig. 8). In the P4 anion the four F atoms of the equatorial plane are disordered over two crystallographic positions each (s.o.f. 0.41 and 0.59). Interestingly, the four independent donors have their ethyl substituents in axial positions, although this situation is extremely rare in radical cation salts of dimethylated and tetramethylated EDT-TTF and BEDT-TTF donors for which the methyl substituents arrange in equatorial position in radical cation salts, in order to maximize the orbital overlap between open-shell species. However, for the diethyl and tetraethyl corresponding donors, the much higher stability of the (ax,ax) conformation with respect to the (eq,eq) one promotes the

occurrence of the former even in radical cation salts in the solid state and not only in the neutral precursors.

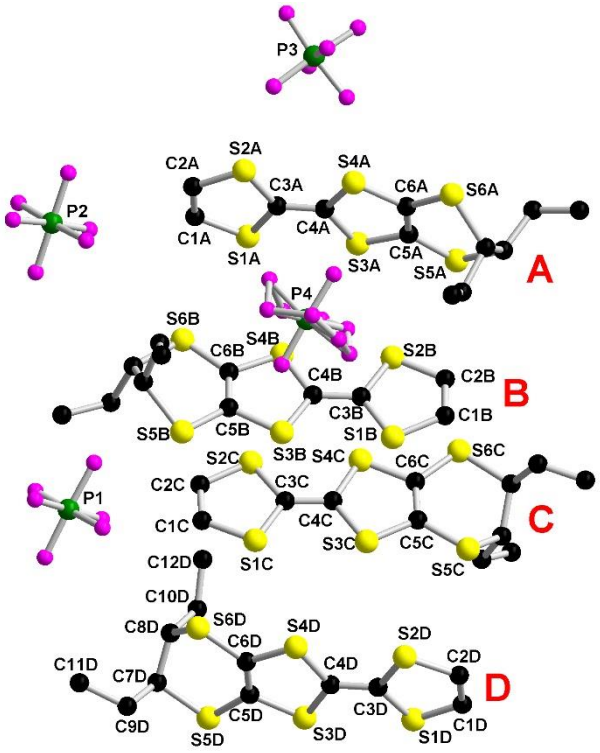

Fig. 8 The four independent donors and anions in the crystal structure of [(*S*)-**1**]PF_6, together with a partial atom numbering scheme. Hydrogen atoms have been omitted for clarity.

Due to the 4:4 stoichiometry, the four independent donors should bear a +1 charge each, in agreement with the values of the central C=C and internal C−S bond distances (Table S5). In the packing the donors form rows of interacting AD and BC dimers along the *c* direction, with very short intradimer S···S distances of 3.36 – 3.41 Å (BC) and 3.32 – 3.48 Å (AD) (Fig. 9). The interdimer S···S distances are much longer, amounting at 3.68 Å (BC) and 3.69 Å (AD). The rows AD and BC are separated along the *b* direction by layers of anions, yet two rather short interchain S···S distances of 3.60 Å can be observed (S2D···S3C and S2B···S5A). Along the *c* direction the donors are interconnected through hydrogen bonds between the fluorine atoms of the anions and the different types of hydrogen atoms of the donors (Fig. S18).

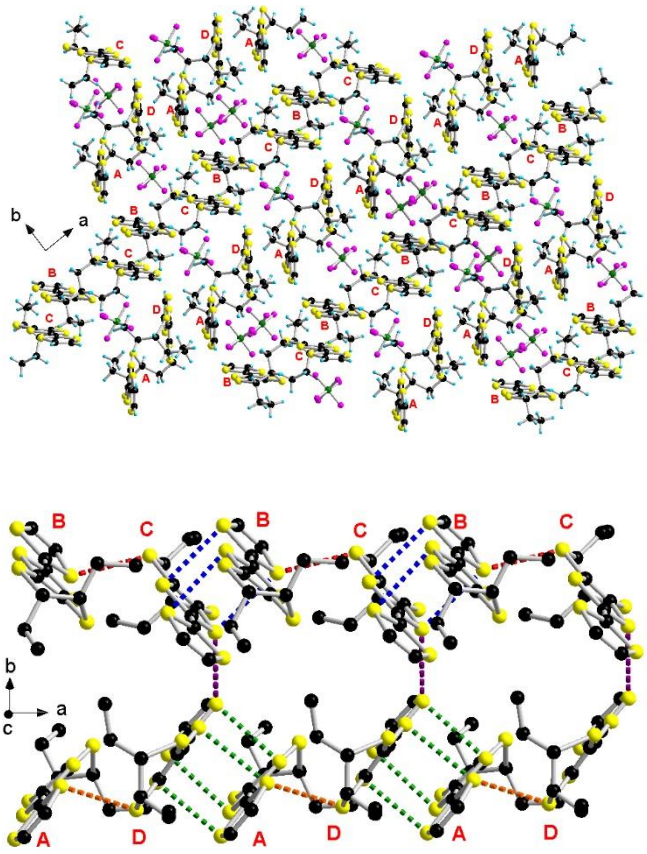

Fig. 9 Packing diagram of [(*S*)-**1**]PF_6 in the *ab* plane (top) with a focus on the short intermolecular S···S contacts highlighted as dotted lines (blue and green for intradimer contacts, red and orange interdimer contacts within the chain and violet for interchain contacts) (bottom).

As mentioned above, no other crystalline radical cation salts based on donors **1** and **2** could be obtained in the course of our attempts. Note that in the only previous report mentioning the use of donor **2** as (*rac*) / (*meso*) mixture in electrocrystallization experiments, three salts have been described.[31] They are formulated as (*rac*/*meso*-**2**)($AuCl_2$)($AuCl_4$), (*meso*-**2**)(IBr_2)$_2$ and (*rac*-**2**)(I_3), thus containing the dication $\mathbf{2}^{2+}$ for the first two and the radical cation $\mathbf{2}^{+\bullet}$ for the last one. Interestingly, in all these salts the ethyl substituents are always located in axial positions, pointing out again the superior stability of the all-ax conformer with respect to the all-eq one. The difficulty of obtaining crystalline radical cation salts based on **1** and **2** when compared to the methylated precursors TM-BEDT-TTF, DM-BEDT-TTF and DM-EDT-TTF (Scheme 1) is very likely related to the higher solubility of the former and also to the propensity of the ethyl substituents to arrange in axial positions, thus hampering an efficient TTF···TTF packing which is the main driving force in the crystallization of TTF based radical cation salts or charge transfer complexes.

Further, we have engaged **1** and **2** in chemical oxidation with the $TCNQF_4$ (tetrafluoro-tetracyano-quinodimethane) donor. The three forms of **1**, i.e. (*rac*), (*S*,*S*) and (*R*,*R*) provided dark crystalline rectangular plates upon evaporation from acetonitrile solutions, yet those of the racemic samples were not well diffracting. The enantiopure charge transfer (CT) complexes crystallized in the triclinic non-centrosymmetric *P*1 space group, showing a 1:1 donor/acceptor stoichiometry. In the following only the structure of [(*R*)-**1**]$TCNQF_4$ will be detailed since the data for the enantiomeric compound were of lesser quality. The asymmetric unit cell consists of four independent donor A-D and four $TCNQF_4$ molecules (Fig. S19). The C=C and C–S internal bond distances values confirm the +1 oxidation state of the donors (Table S6). Interestingly, the ethyl substituents are located in equatorial position in all the four independent donors, in sharp contrast with the previous structures of the neutral **1** and the radical cation salt [(*S*)-**1**]PF_6. Here, probably, the efficient orbital overlap between the $TCNQF_4^{-\bullet}$ radical anion species promotes a tight packing of the donors, triggering the equatorial orientation of the substituents, which overcomes the unfavourable energy difference between the equatorial and axial conformations. Indeed, the $TCNQF_4$ acceptor molecules form eclipsed dimeric units, with very short intradimer C···C contacts of 3.13 – 3.26 Å. These dimers further stack along the *a* direction with either lateral or longitudinal shifts, whereas the DE-EDT-TTF molecules are arranged in dimeric rows A-B and C-D along the *b* direction, perpendicular to the acceptor stacks, thus providing a segregated donor-acceptor architecture (Fig. 10 and S20).

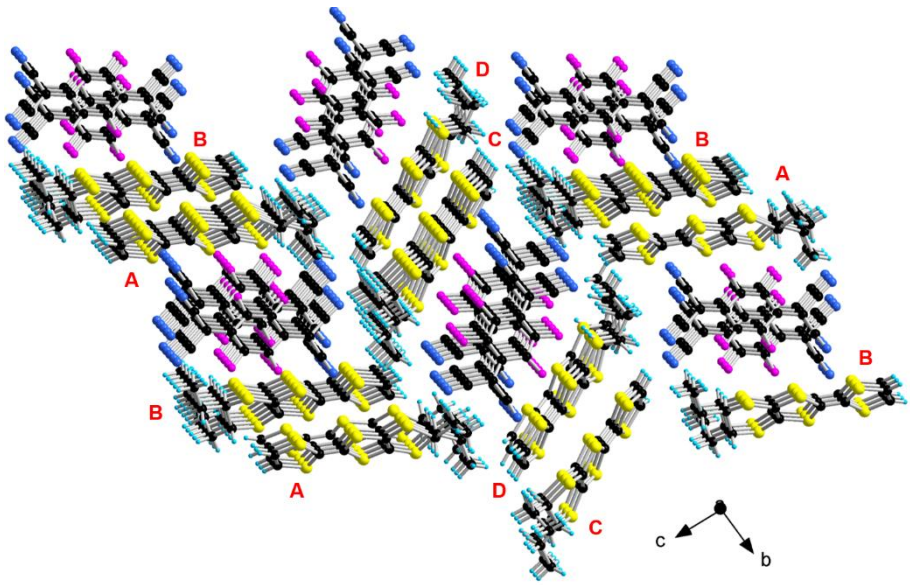

Fig. 10 Packing diagram of [(*R*)-**1**]$TCNQF_4$ in the *bc* plane (top) with a focus on the dimeric rows of donors.

The TTF cores of the donors are practically eclipsed within the A-B and C-D dimers, with very short intermolecular intradimer S···S contacts of 3.31 – 3.37 and 3.33 – 3.45 Å for A-B and C-D, respectively. Longer lateral interdimer S···S distances amounting at 3.73 – 3.87 (A···B) and 3.60 – 3.99 (C···D) Å are observed in the *ab* plane (Fig. 11).

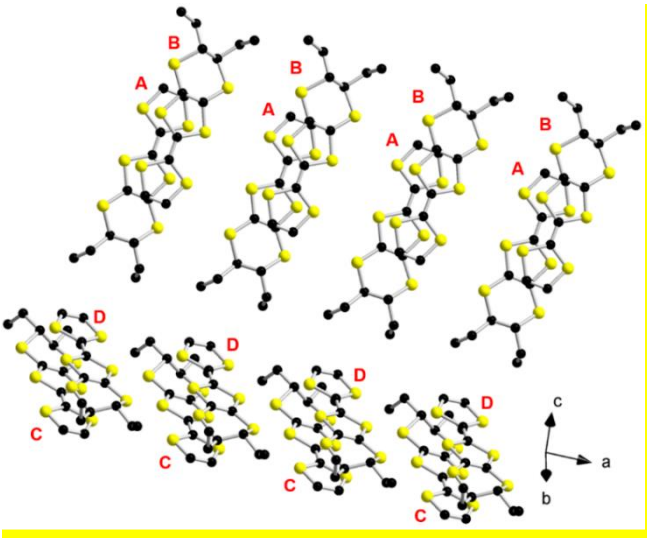

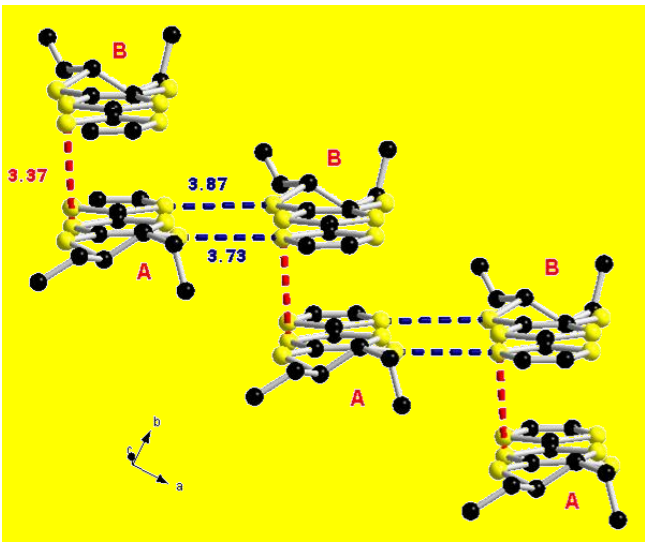

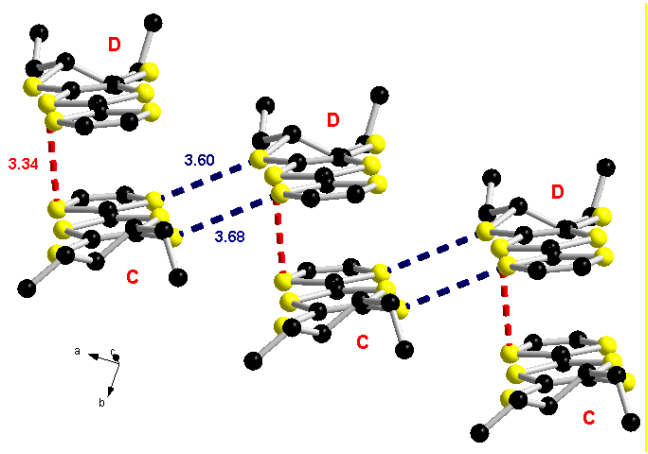

Fig. 11 Dimeric rows of donors in the structure of [(*R*)-**1**]TCNQF$_4$ (top); rows of AB dimers with short S···S contacts (middle); rows of CD dimers with short S···S contacts (bottom).

In contrast to **1**, only the meso form of **2** provided suitable single crystals of a charge transfer complex with TCNQF$_4$ formulated as [(*meso*)-**2**]TCNQF$_4$. The compound crystallized in the centrosymmetric triclinic space group *P*–1, with a half independent molecule of donor and a half independent molecule of acceptor in the asymmetric unit (Fig. S21). The absolute configuration of the four stereogenic centres of the donor is thus (*R*,*R*,*S*,*S*), since the inversion centre is located on the central C=C bond, which has a length value typical for an oxidized donor (Table S7). Unlike the previous charge transfer salt [(*R*)-**1**]TCNQF$_4$ showing a segregated structure, here the donor and acceptor form alternated stacks along the *b* direction, while the donors interact laterally along the *a* direction through S···S intermolecular contacts of 3.58 – 3.63 Å (Fig. 12).

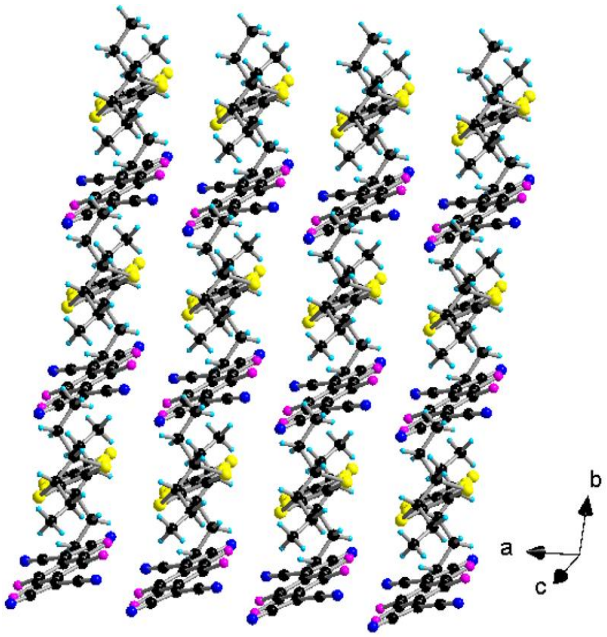

Fig. 12 Packing diagram of [(*meso*)-**2**]TCNQF$_4$ showing the alternated stacks along *b*.

Interestingly, the donors show now an all-axial conformation of the ethyl substituents, probably a consequence of the alternated donor-acceptor pattern. The values of the central C=C and internal C–S bonds (Table S7) suggest a total charge transfer between the donor and the acceptor.

3. Conclusions

Chiral diethyl and tetraethyl substituted EDT-TTF and BEDT-TTF donors **1** and **2**, respectively, have been synthesized as racemic mixtures from the common precursor 5,6-diethyl-5,6-dihydro-1,4-dithiin-2,3-dithiol-thione, and then separated in pure enantiomers by chiral HPLC. The absolute configurations have been determined by a combination of single crystal X-ray diffraction analysis, performed on all the neutral forms, CD spectroscopy and DFT and TD-DFT calculations. Worth noting is the axial conformation of the ethyl substituents in all the solid state structures of **1** and **2**, in agreement with the higher stability of the (ax,ax) conformer of **1** over the (eq,eq) one. In striking contrast with the results on the DM-EDT-TTF and dm-dddt series, the (ax,ax) and (eq,eq) conformers of the same enantiomer of **1** show similar CD theoretical spectra, and thus the equilibrium between the two forms in solution does not impact the experimental CD. Electrocrystallization experiments provided so far only one complete series of crystalline radical cations salts for donor **1**, formulated as (**1**)PF_6, where, once again, the ethyl substituents are arranged in axial positions in all the four independent donors. In sharp contrast, in the charge transfer salt [(*R*)-**1**]$TCNQF_4$, the ethyl substituents are located in equatorial positions, very likely because of the segregated donor-acceptor structure implying a tight packing of the acceptors and, consequently, of the donors. For donor **2**, the charge transfer salt [(*meso*)-**2**]$TCNQF_4$ shows alternated donor-acceptor packing, with the ethyl groups of the donors in axial positions. The easy access to the new two families of chiral TTF donors opens up the possibility to engage them in chiral charge transfer complexes with various acceptors, for example with $TCNQF_2$ instead of $TCNQF_4$, in order to decrease the charge transfer degree. Additionally, the diethyl dithiole-thione intermediate **5** can be used to prepare other families of chiral TTF precursors for chiral conductors. Moreover, chiral metal bis(dithiolene) complexes based on the diethyl-dddt ligand, showing original chiroptical and conducting properties, can be also envisaged.

4. Experimental

4.1 Materials and instrumentation

Reactions were carried out under nitrogen; dry solvents were obtained from distillation machines. Nuclear magnetic resonance spectra were recorded on a Bruker Avance DRX 300 spectrometer operating at 300 MHz for ^1H and 75 MHz for ^{13}C. Chemical shifts are expressed in parts per million (ppm) downfield from external TMS. The following abbreviations are used: s, singlet; d, doublet; dq, doublet of quadruplets; m, massif. MALDI-TOF MS spectra were recorded on a Bruker Biflex-IIITM apparatus, equipped with a 337 nm N_2 laser.

Elemental analysis was performed using a Flash 2000 Fisher Scientific Thermo Electron analyzer.

4.2 Synthesis

The 1,3-dithiolane-2,4,5-trithione **4** has been synthesized according to the published procedure (see the SI).[33]

(*rac*)-5,6-Diethyl-5,6-dihydro-[1,3]dithiolo[4,5-b][1,4]dithiine-2-thione ((*rac*)-5). Trithione **4** (3 g, 0.015 mol) was added into a 250 mL round bottomed flask containing 140 mL of toluene. *Trans*-3-Hexene (3.8 mL, 0.03 mol) was added into the flask and refluxed for four hours at 110 °C. The solvent was then evaporated using a rotary evaporator, and the product was purified by column chromatography using petroleum spirit/dichloromethane 8/2 to afford **5** as a yellowish solid (3.1 g, 74%). ^{1}H NMR (300 MHz, $CDCl_3$) δ ppm: 3.16 (m, 2H, *CH*), 1.92 (m, 4H, CH_2), 1.08 (t, 6H, CH_3). ^{13}C NMR (76 MHz, $CDCl_3$) δ ppm: 208.11(*C*=*S*), 121.06 (*C*=*C*), 49.26 (*CH*), 29.65(CH_2), 11.38 (CH_3). MS (EI) *m/z*: 280.96 (M_{th} = 279.95)

(*rac*)-DE-EDT-TTF-(COOMe)$_2$ ((*rac*)-7). Compound **5** (2 g, 7.1 mmol) and dimethyl-2-oxo-1,3-dithiole-4,5-dicarboxylate **6** (3.3g, 14 mmol) were mixed under argon in freshly distilled trimethyl phosphite (20 mL), and the mixture was heated at 110 °C for 5 h. The solvent was evaporated in a rotary evaporator, and then toluene (40 mL) was added and evaporated. The last procedure was repeated twice. The product was solubilized in dichloromethane and passed down a silica column to remove the remaining phosphite and then purified by chromatography using petroleum spirit/dichloromethane 1/1 to afford a red-brown solid (1.3 g, 58 %). ^{1}H NMR (300 MHz, $CDCl_3$) δ ppm: 3.85 (s, 6H, -OCH_3), 3.05 (t, *J* = 5.7 Hz, 2H, *CH*), 1.76 (m, 4H, CH_2), 1.05 (t, *J* = 7.3 Hz, 6H, CH_3). ^{13}C NMR (75 MHz, $CDCl_3$) δ ppm: 159.8 (*C*=O), 131.6, 111.9, 110.4, 110.1 (*C*=*C*), 53.1 (O-CH_3), 49.2 (*CH*), 29.6 (CH_2), 11.3 (CH_3). MS (MALDI-TOF) *m/z*: 465.96 (M_{th} = 465.95).

(*rac*)/(*meso*)-TE-BEDT-TTF ((*rac/meso*)-2). The compound **2**, as a (*rac*)/(*meso*) mixture, resulted from the same coupling reaction as **7** following a homo-coupling route between 2 equivalents of **6**, and has been eluted before **7**. Its spectroscopic characteristics were in agreement with the published data.[31]

(*rac*)-DE-EDT-TTF ((*rac*)-1). Compound **7** (1 g, 2.1 mmol) and LiBr (2.6 g, 30 mmol, 14 eq.) were mixed in dimethylformamide (100 mL). The solution was stirred at 150 °C for 30 min, the formation of the product being monitored by TLC. The product was extracted with dichloromethane, and the organic phase was washed with brine and water and then dried over $MgSO_4$. The solvent was removed under a vacuum, and the product was purified by chromatography on a silica gel column with petroleum spirit/dichloromethane 6/4 to afford a red solid (0.29 g, 35%). ^{1}H NMR (300 MHz, $CDCl_3$) δ ppm: 6.32 (s, 2H, $CH_{vinylic}$), 3.03 (m, 2H, *CH*), 1.92 – 1.64 (m, 4H, CH_2), 1.05 (t, J = 7.3 Hz, 6H, CH_3). ^{13}C NMR (76 MHz, $CDCl_3$) δ ppm: 119.08, 117.73, 111.97, 104.37 (*C=C*), 50.02 (*CH*), 29.45 (CH_2), 11.57 (CH_3). MS (EI) m/z: 394.94 (M_{th} = 394.94). Elemental analysis calcd. (%) for $C_{12}H_{14}S_6$: C 41.11, H 4.03, S 54.87; found: C 40.76, H 3.82, S 55.17.

Charge transfer salts with $TCNQF_4$. (*rac*), (*S*) and [(*R*)-**1**]$TCNQF_4$ were prepared by adding a $TCNQF_4$ solution to the donor solution in acetonitrile in a 1:1 stoichiometry, then rectangular plates were recovered by slow evaporation after 10 days. [(*meso*)-**2**]$TCNQF_4$ was prepared by the same procedure.

4.3 Electrocrystallization

[(*rac*)-1]PF_6. 20 mg of $[NBu_4]PF_6$ was dissolved in THF (6 mL), and then the solution was poured into the cathodic compartment of an electrocrystallization cell. The anodic chamber was filled with 5 mg of (*rac*)-**1** dissolved in THF (6 mL). Crystalline black rectangular plates of the salt [(*rac*)-**1**]PF_6 were grown at 20° C over a period of two weeks on the platinum wire electrode, by applying a constant current of 2 µA.

[(*S*)-1]PF_6. Prepared as previously by using (*S*)-**1** as precursor.

[(*R*)-1]PF_6. Prepared as previously by using (*R*)-**1** as precursor.

4.4 X-Ray structure determinations

Details about data collection and solution refinement are given in Tables S1 and S2. Single crystals of the compounds were mounted on glass fibre loops using a viscous hydrocarbon oil to coat the crystal and then transferred directly to cold nitrogen stream for data collection. X-ray data collections were performed at room temperature or at 150 K on a Rigaku Oxford Diffraction SuperNova diffractometer equipped with an Atlas CCD detector and micro-focus Cu-K_α radiation (λ = 1.54184 Å). The structures were solved by direct methods or dual-space algorithm

and refined on F^2 by full matrix least-squares techniques with SHELX programs (SHELXS-2013 or SHELXT-2018 and SHELXL-2016-2018)[34,35] using the WinGX graphical user interface.[36] All non-H atoms were refined anisotropically. Hydrogen atoms were introduced at calculated positions (riding model), included in structure factor calculations but not refined. Crystallographic data for the ten structures have been deposited with the Cambridge Crystallographic Data Centre, deposition numbers CCDC 2179911 ((*rac*)-**1**), 2179912 ((*S*)-**1**), 2179913 ((*R*)-**1**), 2179914 ([(*S*)-**1**]PF_6), 2179915 ([(*R*)-**1**]$TCNQF_4$), 2179916 ((*rac*)-**2**), 2179917 ((*S*)-**2**), 2179918 ((*R*)-**2**), 2179919 ((*meso*)-**2**), 2179920 ([(*meso*)-**2**]$TCNQF_4$). These data can be obtained free of charge from CCDC, 12 Union road, Cambridge CB2 1EZ, UK (e-mail: deposit@ccdc.cam.ac.uk or http://www.ccdc.cam.ac.uk).

4.5 DFT and TD-DFT calculations

For all calculations, the Gaussian 09 software (revision D.01) has been used.[37] All ground states in gas phase have been optimized by a DFT approach with the PBE1PBE hybrid functional and the 6–311+G(3df,2pd) basis set.[38] Then, frequency calculations confirmed that all optimized geometries correspond to global minima in the potential energy surface. A Time-Dependent DFT method has been employed to compute the first 40 excited singlet states with the same level of theory. The theoretical UV-visible absorption spectra have been simulated by Gaussian broadening of the calculated transition energies (FWHM of 3000 cm^{-1}). The full molecular reports, molecular orbitals, electron density differences pictures and spectra have been automatically generated by a homemade Python program, quchemreport, based on cclib.[39,40]

Author Contributions

N.M. synthesized and characterized the compounds, performed the electrocrystallization and chemical oxidation experiments and the X-Ray measurements. T.C. undertaken the DFT calculations and interpreted the results. N.V. performed the chiral HPLC separation of the compounds. N.A. supervised the project and wrote and revised the manuscript with inputs from all the co-authors.

Conflicts of interest

There are no conflicts to declare.

Acknowledgements

This work was supported by the National Agency for Research (ANR, Project 15-CE29-0006-01 ChiraMolCo), the CNRS and the University of Angers. Ingrid Freuze and Sonia Jerjir (University of Angers) are gratefully acknowledged for MS characterization, and Magali Allain (University of Angers) for help with some of the X-ray structures.

Notes and references

1 F. Pop, N. Zigon and N. Avarvari, *Chem. Rev.*, 2019, **119**, 8435–8478.

2 G. L. J. A. Rikken, J. Fölling and P. Wyder, *Phys. Rev. Lett.*, 2001, **87**, 236602.

3 C. Réthoré, N. Avarvari, E. Canadell, P. Auban-Senzier and M. Fourmigué, *J. Am. Chem. Soc.*, 2005, **127**, 5748–5749.

4 A. M. Madalan, C. Réthoré, M. Fourmigué, E. Canadell, E. B. Lopes, M. Almeida, P. Auban-Senzier and N. Avarvari, *Chem. Eur. J.*, 2010, **16**, 528–537.

5 F. Pop, P. Auban-Senzier, A. Frąckowiak, K. Ptaszyński, I. Olejniczak, J. D. Wallis, E. Canadell and N. Avarvari, *J. Am. Chem. Soc.*, 2013, **135**, 17176–17186.

6 F. Pop, P. Auban-Senzier, E. Canadell and N. Avarvari, *Chem. Commun.*, 2016, **52**, 12438–12441.

7 R. Naaman, Y. Paltiel and D. H. Waldeck, *Nat. Rev. Chem.*, 2019, **3**, 250–260.

8 P. Chandra Mondal, N. Kantor-Uriel, S. P. Mathew, F. Tassinari, C. Fontanesi and R. Naaman, *Adv. Mater.*, 2015, **27**, 1924–1927.

9 A. Inui, R. Aoki, Y. Nishiue, K. Shiota, Y. Kousaka, H. Shishido, D. Hirobe, M. Suda, J. Ohe, J. Kishine, H. M. Yamamoto and Y. Togawa, *Phys. Rev. Lett.*, 2020, **124**, 166602.

10 F. Pop and N. Avarvari, *Coord. Chem. Rev.*, 2017, **346**, 20–31.

11 N. Avarvari and J. D. Wallis, *J. Mater. Chem.*, 2009, **19**, 4061–4076.

12 J. D. Dunitz, A. Karrer and J. D. Wallis, *Helv. Chim. Acta*, 1986, **69**, 69–70.

13 S. Matsumiya, A. Izuoka, T. Sugawara, T. Taruishi and Y. Kawada, *Bull. Chem. Soc. Jpn.*, 1993, **66**, 513–522.

14 A. Karrer, J. D. Wallis, J. D. Dunitz, B. Hilti, C. W. Mayer, M. Bürkle and J. Pfeiffer, *Helv. Chim. Acta*, 1987, **70**, 942–953.

15 S. Yang, F. Pop, C. Melan, A. C. Brooks, L. Martin, P. Horton, P. Auban-Senzier, G. L. J. A. Rikken, N. Avarvari and J. D. Wallis, *CrystEngComm*, 2014, **16**, 3906–3916.

16 J. R. Galán-Mascarós, E. Coronado, P. A. Goddard, J. Singleton, A. I. Coldea, J. D. Wallis, S. J. Coles and A. Alberola, *J. Am. Chem. Soc.*, 2010, **132**, 9271–9273.

17 F. Riobé, F. Piron, C. Réthoré, A. M. Madalan, C. J. Gómez-García, J. Lacour, J. D. Wallis and N. Avarvari, *New J. Chem.*, 2011, **35**, 2279–2286.

18 F. Pop, S. Laroussi, T. Cauchy, C. J. Gómez-García, J. D. Wallis and N. Avarvari, *Chirality*, 2013, **25**, 466–474.

19 M. Atzori, F. Pop, P. Auban-Senzier, R. Clérac, E. Canadell, M. L. Mercuri and N. Avarvari, *Inorg. Chem.*, 2015, **54**, 3643–3653.

20 F. Pop, P. Batail and N. Avarvari, *Crystals*, 2016, **6**, 8.

21 F. Pop, C. Mézière, M. Allain, P. Auban-Senzier, N. Tajima, D. Hirobe, H. M. Yamamoto, E. Canadell and N. Avarvari, *J. Mater. Chem. C*, 2021, **9**, 10777–10786.

22 S. Matsumiya, A. Izuoka, T. Sugawara, T. Taruishi, Y. Kawada and M. Tokumoto, *Bull. Chem. Soc. Jpn.*, 1993, **66**, 1949–1954.

23 F. Pop, M. Allain, P. Auban-Senzier, J. Martínez-Lillo, F. Lloret, M. Julve, E. Canadell and N. Avarvari, *Eur. J. Inorg. Chem.*, 2014, 3855–3862.

24 J. S. Zambounis, C. W. Mayer, K. Hauenstein, B. Hilti, W. Hofherr, J. Pfeiffer, M. Bürkle and G. Rihs, *Adv. Mater.*, 1992, **4**, 33–35.

25 N. Mroweh, C. Mézière, F. Pop, P. Auban-Senzier, P. Alemany, E. Canadell and N. Avarvari, *Adv. Mater.*, 2020, **32**, 2002811.

26 N. Mroweh, C. Mézière, M. Allain, P. Auban-Senzier, E. Canadell and N. Avarvari, *Chem. Sci.*, 2020, **11**, 10078–10091.

27 F. Pop, P. Auban-Senzier, E. Canadell, G. L. J. A. Rikken and N. Avarvari, *Nat. Commun.*, 2014, **5**, 3757.

28 N. Mroweh, P. Auban-Senzier, N. Vanthuyne, E. Canadell and N. Avarvari, *J. Mater. Chem. C*, 2019, **7**, 12664–12673.

29 N. Mroweh, P. Auban-Senzier, N. Vanthuyne, E. B. Lopes, M. Almeida, E. Canadell and N. Avarvari, *Crystals*, 2020, **10**, 1069.

30 N. Mroweh, A. Bogdan, F. Pop, P. Auban-Senzier, N. Vanthuyne, E. B. Lopes, M. Almeida and N. Avarvari, *Magnetochemistry*, 2021, **7**, 87.

31 A. M. Kini, J. P. Parakka, U. Geiser, H.-H. Wang, F. Rivas, E. DiNino, S. Thomas, J. D. Dudek and J. M. Williams, *J. Mater. Chem.*, 1999, **9**, 883–892.

32 T. Cauchy, F. Pop, J. Cuny and N. Avarvari, *Chimia*, 2018, **72**, 389–393.

33 N. Svenstrup and J. Becher, *Synthesis*, 1995, **1995**, 215–235.

34 G. M. Sheldrick, *Acta Cryst.*, 2015, **C71**, 3–8.

35 G. M. Sheldrick, *Acta Cryst.*, 2015, **A71**, 3–8.

36 L. J. Farrugia, *J. Appl. Cryst.*, 2012, **45**, 849–854.

37 M. J. Frisch, G. W. Trucks, H. B. Schlegel, G. E. Scuseria, M. A. Robb, J. R. Cheeseman, G. Scalmani, V. Barone, B. Mennucci, G. A. Petersson, H. Nakatsuji, M. Caricato, X. Li, H. P. Hratchian, A. F. Izmaylov, J. Bloino, G. Zheng, J. L. Sonnenberg, M. Hada, M. Ehara, K. Toyota, R. Fukuda, J. Hasegawa, M. Ishida, T. Nakajima, Y. Honda, O. Kitao, H. Nakai, T. Vreven, J. A.

Montgomery Jr., J. E. Peralta, F. Ogliaro, M. Bearpark, J. J. Heyd, E. Brothers, K. N. Kudin, V. N. Staroverov, R. Kobayashi, J. Normand, K. Raghavachari, A. Rendell, J. C. Burant, S. S. Iyengar, J. Tomasi, M. Cossi, N. Rega, J. M. Millam, M. Klene, J. E. Knox, J. B. Cross, V. Bakken, C. Adamo, J. Jaramillo, R. Gomperts, R. E. Stratmann, O. Yazyev, A. J. Austin, R. Cammi, C. Pomelli, J. W. Ochterski, R. L. Martin, K. Morokuma, V. G. Zakrzewski, G. A. Voth, P. Salvador, J. J. Dannenberg, S. Dapprich, A. D. Daniels, Ö. Farkas, J. B. Foresman, J. V. Ortiz, J. Cioslowski and D. J. Fox, *Gaussian~09 Revision D.01*.

38 C. Adamo and V. Barone, *J. Chem. Phys.*, 1999, **110**, 6158–6170.

39 N. M. O'boyle, A. L. Tenderholt and K. M. Langner, *J. Comput. Chem.*, 2008, **29**, 839–845.

40 T. Cauchy and B. Da Mota, *quchemreport. A python program for control quality and automatic generation of quantum chemistry results*, University of Angers, 2020.